Sensors & Diagnostics

ROYAL SOCIETY
OF CHEMISTRY

PAPER

Open Access Article. Published on 09 July 2024. Downloaded on 2/11/2026 10:39:29 AM. This article is licensed under a Creative Commons Attribution 3.0 Unported Licence.

View Article Online
View Journal | View Issue

Cu²⁺-integrated carbon dots as an efficient bioprobe for the selective sensing of guanine nucleobase†

Monalisa Chowdhury, Debolina Basu and Prasanta Kumar Das 🆔 *

This present work aimed to craft copper (Cu²⁺)-doped carbon dots (CuCDs) for the selective and sensitive detection of a guanine nucleobase. By employing a hydrothermal method, we synthesized blue-emitting CuCDs having emission maxima at 423 nm. CuCDs were used as a fluorescence turn-on ratiometric probe to detect guanine, a critical purine base in DNA involved in energy transduction, cell signalling, and metabolic processes. In the presence of guanine, the fluorescence intensity of CuCDs significantly increased due to the stable non-covalent interaction between Cu²⁺ and guanine. CuCDs achieved a very low limit of detection (LOD) of 0.59 nM for guanine as a highly sensitive probe. CuCDs demonstrated selectivity for guanine with no interference from other nucleobases (adenine, thymine, and cytosine) and various biomolecules and metal ions commonly found in the cellular environment. In addition, CuCDs demonstrated a higher affinity for guanine-enriched oligonucleotide cMYC G 27-mer over dsDNA 26-mer devoid of a large guanine population. Furthermore, the fluorescence intensity of CuCDs increased in guanine-treated mammalian cells and G-quadruplex-enriched cancer cells compared with that in non-cancerous cells. Hence, we developed a highly sensitive ratiometric fluorescence probe, CuCDs, for the selective detection of guanine both in vitro and within mammalian cells via a "fluorescence turn-on mechanism".

Received 30th April 2024,
Accepted 4th July 2024

DOI: 10.1039/d4sd00137k

rsc.li/sensors

Introduction

The human chromosome, a complex biopolymer, houses DNA that encodes the genetic blueprint crucial for life processes and protein biosynthesis.[1–4] The nucleotides of DNA, i.e. guanine (G), adenine (A), thymine (T), and cytosine (C),[5–7] facilitate the replication and transcription of genetic information. Guanine is vital for energy transduction, cell signalling, and metabolic cofactors.[8–10] However, guanine is prone to oxidation, with its product 8-oxo-Gua serving as a biomarker for oxidative stress and DNA damage. Changes in guanine levels can lead to immune system deficiencies and diseases such as liver disease, AIDS, renal calculi, and cancer, highlighting the need for effective guanine detection methods.[8,11–16] Techniques such as laser-induced

fluorimetry,[17] chromatography,[18] capillary electrophoresis,[19] high-performance liquid chromatography (HPLC),[20,21] and mass spectrometry (MS)[22] are used for guanine detection; however, they face challenges such as complex sample preparation and poor reproducibility.[4,23,24] Fluorometric sensing is promising due to its simplicity, cost-effectiveness, and high sensitivity.[25,26] Although various nanomaterials have been explored for this purpose (including metal nanoparticles, semiconductor-based quantum dots, and dye-doped materials),[27–29] they have limitations such as toxicity and low photostability.[30,31] Hence, there is an urgent demand for the development of simple, sensitive, and selective biosensors for guanine for both in vitro and in vivo applications.

In the field of biosensing, carbon dots (CDs) have garnered considerable attention by representing a novel category of zero-dimensional carbon-based nanomaterials with diameters under 10 nm. CDs are recognized for their unique inherent fluorescence properties, cytocompatibility, facile synthesis, high photostability, water solubility, and chemical inertness.[32–36] In carbon dots, surface defects play a crucial role in their optical properties. Upon photoexcitation, rapid charge separation occurs, resulting in the generation of electrons and holes. These charge carriers become trapped at various surface sites, leading to radiative recombination and

School of Biological Sciences, Indian Association for the Cultivation of Science, Jadavpur, Kolkata – 700032, India. E-mail: bcpkd@iacs.res.in

† Electronic supplementary information (ESI) available: Synthetic schemes, high-resolution FEGTEM images of CuCD, DLS study, deconvoluted spectra of C 1s, O 1s, N 1s, XRD and EDX of CuCD, Tauc's plot, Stern–Volmer plot, structure of nucleobases, proposed binding model of CuCD-guanine complex, Stern–Volmer plot, interference study, FEGTEM image of CuCD-guanine complex, stability index of CuCD, cytocompatibility of CuCD, bioimaging of guanine-treated CuCD-incubated NIH3T3 cells. See DOI: https://doi.org/10.1039/d4sd00137k

© 2024 The Author(s). Published by the Royal Society of Chemistry

Sens. Diagn., 2024, 3, 1329–1343 | 1329

the emission of light, which is a characteristic of carbon dots.[37–39]

In the last decade, researchers have been intrigued by nucleobase sensing, as DNA, the fundamental genetic material, comprises nucleobases (A, T, G, and C). Guanine, as discussed above, is of particular interest due to its implications under conditions such as cancer and AIDS. Researchers have used electrochemical and fluorescence methods, employing diverse tools such as quantum dots, polymers, conjugates, carbon nanotubes, and nanocapsules, to detect guanine. For example, intrinsic dual emitting ZnCdTe QDs were synthesized to selectively sense guanine having LOD 0.076 μmol L^{-1};[23] TiO$_2$-graphene nanocomposite was prepared by in situ hydrothermal treatment, where the electrochemical behavior of adenine and guanine at the TiO$_2$-graphene nanocomposite modified glassy carbon electrode was investigated.[40] The MgO nanoparticles (NPs) were prepared in a mechanochemical manner, and magnesium oxide and multi-walled carbon nanotubes modified carbon paste electrode (MgO-MWCNTs-MCPE) were utilized for the specific and simultaneous investigation of guanine, adenine and epinephrine using an electrochemical method.[10] Surface assembly of poly(9-(2-diallylaminoethyl) adenineHCl-co-sulfurdioxide) (polyA) on silica nanoparticles form nanocapsules, which selectively sensed guanine over other nucleobases using the conjugation with curcumin.[41] However, each method has limitations, such as low selectivity, the toxicity of metal-based bioprobes, and short sensor lifespans.

Considering these attributes, herein, we aim to develop copper (Cu^{2+})-doped carbon dots (CuCDs) for the selective and sensitive detection of guanine nucleobase. Previous reports suggest that the specific arrangement of oxygen at C6 and N7 in guanine facilitates optimal interaction with Cu^{2+} ions rather than other nucleobases. Considering this fact, we harnessed the blue-emission (emission maxima at 423 nm) of CuCDs prepared using the hydrothermal method. The CuCD was employed as a fluorescent turn-on bioprobe for the simple, sensitive, and selective detection of guanine. The fluorescence intensity of CuCDs significantly increased in the presence of guanine, which is attributed to the stable interaction between Cu^{2+} and guanine. CuCDs serve as a highly sensitive fluorescence probe for guanine with a limit of detection (LOD) of 0.59 nM. Importantly, guanine sensing by CuCDs demonstrates selectivity in solution against other nucleobases, i.e. adenine, thymine, cytosine and various biomolecules and metal ions abundant in the cellular environment with no interference. Notably, the fluorescence intensity of cytocompatible (up to 85%) CuCDs increased in guanine-enriched (B16F0, MCF-7) and guanine-treated mammalian cells (NIH3T3) compared to untreated NIH3T3 cells. Thus, we developed a highly sensitive ratiometric fluorescent probe, CuCD, for the selective detection of guanine through a "fluorescence turn-on mechanism".

Experimental section

Materials

Ethylenediaminetetraacetic acid disodium salt (EDTA-2Na, 2H$_2$O; purity ≥ 98.0%), copper chloride dihydrate (CuCl$_2$·2H$_2$O; purity ≥ 98.5%), adenine (A), guanine (G), cytosine (C), thymine (T) (all nucleobase having purity ≥ 98.0%) NaCl (purity ≥ 99.0%), KCl (purity ≥99.5%), CaCl$_2$·2H$_2$O (purity ≥ 98.0%), FeCl$_2$·2H$_2$O (purity ≥ 98.0%), ZnCl$_2$·2H$_2$O (purity ≥ 95.0%), L-cysteine (purity ≥ 99.0%), L-tryptophan (purity ≥ 99.0%), L-tyrosine (purity ≥ 99.0%), L-arginine (purity ≥ 99.0%), L-aspartic acid (purity ≥ 99.0%), GSH (purity ≥ 99.5%), H$_2$O$_2$ (purity ≥ 98.0%) and all other reagents and solvents were bought from SRL, India. cMYC G 27-mer (DTGGGGAGGGTG GGGAGGGTGGGGAAGG) and dsDNA 26-mer (DCAATCGGATCG AATTCGATCCGATTG) DNA sequences, MTT (3-(4,5-dimethylthiazol-2-yl)-2,5-diphenyltetrazolium bromide), and other deuterated solvents were purchased from Sigma-Aldrich. Dialysis tubing was procured from Thermo Scientific SnakeSkin (3.5 K MWCO). Dulbecco's modified Eagle's medium (DMEM), fetal bovine serum (FBS), and trypsin-ethylenediaminetetraacetic acid (EDTA) solution 1× (0.25% solution) were bought from Himedia. NIH3T3, B16F10 and MCF-7 cells were received from NCCS, Pune, India. All experiments were carried out using Milli-Q water. Perkin Elmer Spectrum 100 was used to record FTIR spectra. Centrifugation was performed using a Thermo Scientific Espresso centrifuge. Nano-ZS of Malvern Instruments Limited was used to measure zeta potential. A Telsonic bath sonicator was used to perform bath sonication.

Synthesis of Cu^{2+}-doped carbon dot (CuCD)

A carbon dot doped with Cu^{2+} (CuCD) was prepared using the hydrothermal synthesis approach. Initially, 10 mmol of ethylenediaminetetraacetic acid disodium salt (EDTA-2Na, 2H$_2$O) and 10 mmol of dihydrated copper chloride (CuCl$_2$·2H$_2$O) were dissolved in 10 mL of Milli-Q water. The solution was stirred for 1 h, and the undissolved particles in the mixture were removed through filtration. The remaining solution underwent heating at 190 °C for 5 h in an autoclave Teflon chamber. The mixture was then allowed to cool to room temperature and centrifuged at 13 000 rpm for 10 min. The obtained product was subjected to drying using a freeze dryer, affording CuCD powder with an estimated yield of around 80%. For the control experiments, we prepared another two carbon dots by taking 1 : 2 molar ratio and 2 : 1 molar ratio of EDTA-2Na, 2H$_2$O, and CuCl$_2$·2H$_2$O using identical experimental conditions.

Characterization

The aqueous solution of CuCDs was sonicated for a few minutes, followed by drop casting onto a grid coated with copper and drying. This was then used for examination in an EFGTEM (Transmission electron microscope, 2100F UHR microscope JEOL JEM). For the CuCD-guanine complex, first, the CuCD was sonicated for few minutes. Then, guanine was

added to the **CuCD** for complex formation. Finally, the mixture was drop cast onto a grid and dried overnight before imaging. For atomic force microscopic (AFM) imaging, a drop of **CuCD** solution was air-dried on a fresh mica surface overnight and observed in an Asylum Research MFP-3D microscope in noncontact mode. In the case of X-ray photoelectron spectroscopy (XPS) (Omicron series 0571), rectangular glass plates were utilized to air-dry 8 μL of **CuCD** overnight. EDX (Energy-dispersive X-ray) analysis was performed using an Oxford EXTREME INCA microscope. For XRD (X-ray diffraction), the aqueous **CuCD** solutions (1 mg mL^{-1}) were separately deposited over a glass slide and dried to prepare a thin film, and the spectra were acquired using a diffractometer (Bruker D8 Advance). The mean hydrodynamic diameter (D_h) of the **CuCD** was measured by dynamic light scattering (DLS) (Malvern Zetasizer S90 series) by dissolving 1 mg of lyophilized samples in 1 mL of deionized water. Zeta (ζ) potential measurement was conducted at room temperature using aqueous solutions of the **CuCD**. The UV-visible spectrum of the **CuCD** was measured using Agilent Cary 60, and an Agilent Cary Eclipse luminescence spectrometer was used to record the fluorescence spectra.

Quantum yield (QY) measurement

The absorbance of the carbon dot solution was constrained to less than 0.1 to minimize the inner filter effect, and the integrated emission intensities of these solutions were measured using a luminescence spectrometer. The relative quantum yield (QY) was determined using the following equation:

$$QY = QS \times \frac{I_u}{I_{st}} \times \frac{A_{st}}{A_u} \times \frac{n_u^2}{n_{st}^2}, \qquad (1)$$

where the integrated intensities of the emission spectra for the standard sample (s) and the unknown sample (u) are I_{st} and I_u, respectively; A_{st} and A_u are the absorbances at excitation wavelength for the standard sample (st) and the unknown sample (u), respectively; and the average refractive index values in the wavelength range to calculate the area of fluorescence spectrum for the standard sample (st) and the unknown (u) sample are n_{st} and n_u, respectively. For the determination of QY, standard solutions and unknown solutions with similar absorbance (<0.1) were used, and the same solvent, that is 0.1 M sulfuric acid, was used for the equal refractive index. Quinine sulfate in sulfuric acid (0.1 M) was used as the reference with QY (QS) = 54.0%.

Fluorescence spectroscopy

Fluorescence spectra were recorded for 500 μg mL^{-1} of the **CuCD** by varying the excitation wavelength (λ_{ex}) from 310 to 380 nm. Variation in the fluorescence of the **CuCD** (250 μg mL^{-1}) was investigated in the presence of different concentrations of guanine nucleobase (0–20 nM). All sensing experiments were conducted in Milli-Q water. The Stern–

Volmer constant (K_{SV}) for the fluorescence enhancement of the **CuCD** with respect to the guanine concentration was determined using the equation $F/F_0 = 1 + K_{SV}[Q]$, where F and F_0 represent the fluorescence intensities of the **CuCD** in the presence and absence of guanine, respectively; and [Q] denotes the guanine concentration. The guanine detection limit was assessed from the linear curve obtained from ($F - F_0$)/F_0 versus the guanine concentration. Fluorescence intensity was measured at 423 nm for the **CuCD** upon excitation at 350 nm.

In the selectivity study, the fluorescence of the **CuCD** was investigated in the presence of A, T, and C (500 nM); ions, such as Na$^+$, K$^+$, Ca^{2+}, Fe^{2+}, and Zn^{2+}; and amino acids L-cys, L-tryp, L-tyr, L-arg, L-asp, GSH and H$_2$O$_2$, each with a concentration of 500 nM. In addition, an interference study was performed in which the selective sensing of the guanine (20 nM) nucleobase by the **CuCD** (250 μg mL^{-1}) was studied in the presence of A, T, and C (20 nM). Additionally, the fluorescence response of the **CuCD** (250 μg mL^{-1}) was further examined in the presence of a guanine-enriched oligonucleotide sequence cMYC G 27mer (0.1–1.0 nM) (DTGGGGAGGGTGGGGAGGGTGGGGAAGG). The selectivity of the **CuCD** fluorescence probe in the presence of guanine-enriched sequence was verified through a selectivity study using the guanine-enriched oligonucleotide (cMYC G 27mer) (500 pM or 0.5 nM) against a control oligonucleotide (dsDNA 26mer) (DCAATCGGATCGAATTCGATCCGATTG) (1.0 nM) with limited presence of guanine nucleobase.

FTIR study

FTIR (Fourier-transform infrared) measurements were conducted for the **CuCD** and **CuCD** in conjunction with a guanine-enriched oligonucleotide (cMYC G 27mer) in D$_2$O. Potassium bromide (KBr) was employed to blend with the samples, and a hydraulic press was utilized to form granules. The spectral range extended from 400 to 4000 cm^{-1}, and the spectra underwent normalization and scaling. The experiments were carried out using a Perkin Elmer Spectrum 100 FTIR spectrometer equipped with a 1 mm CaF$_2$ cell.

Media stability of CuCD

The stability of 500 μg mL^{-1} aqueous solutions of the **CuCD** in biological media was assessed using DMEM media with FBS, with concentrations ranging from 0% to 75%. Additionally, the **CuCD** (500 μg mL^{-1}) was exposed to a DMEM with FBS (10%) to examine its stability over a period of 10 days. Supernatants were collected at various time moments, and the absorbance at 365 nm was measured to calculate the suspension stability index (SSI)

$$SSI = A_t/A_0 \times 100, \qquad (2)$$

where A_t = absorbance of the solution after a specific time at 365 nm, and A_0 = initial absorbance of the solution at 365 nm.

Cell culture

NIH3T3, B16F10 and MCF-7 cells were cultured in a medium consisting of DMEM supplemented with 10% FBS and antibiotics (streptomycin and penicillin). The cell cultures were maintained in an incubator at 37 °C with 5% CO_2. After incubation, trypsinization was carried out every 3 days when the cell confluence reached 80%. The trypsinized cells were then utilized for subsequent studies.

Cell viability

The cell viability of the **CuCD** in both cancer and non-cancer cells was assessed using the MTT assay. B16F10, MCF-7 and NIH3T3 cells were separately cultivated in a 96-well plate for 24 h in filtered media. Subsequently, the **CuCD** (25–200 μg mL^{-1}) was incubated for 12 h in the cells (under 5% CO_2 at 37 °C). Following the incubation period, the MTT dye was added and incubated for 4 h. In the MTT assay method, mitochondrial dehydrogenase of living cells generated hydrophobic formazan from the tetrazolium salt. The absorbance of formazan at 570 nm was then measured using a Biotek Elisa Reader, and this absorbance corresponded with the number of viable cells

The number of alive cells was expressed as percent viability
$$= (A_{570}(\text{treated cells}) - \text{background})/A_{570}(\text{untreated cells}) - \text{background}) \times 100. \tag{3}$$

Bioimaging

Non-cancerous NIH3T3 cells and cancer B16F10 and MCF-7 cell lines were cultured (1×10^4 cells per well) in a chamber slide. Initially, guanine (500 nM) was added separately to the chamber slides of NIH3T3 cells for 12 h incubation. Subsequently, the guanine-treated NIH3T3, untreated NIH3T3, and G-quadruplexes (G4s) enriched B16F10, MCF-7 cell lines were washed three times with PBS buffer (pH = 7.4). Next, the **CuCD** (200 μg mL^{-1}) was separately introduced to the chamber slides of all types of cell lines, encompassing control wells and those previously incubated with guanine. For fixation, 4% paraformaldehyde solution was applied for 30 min and mounting was performed using 50% glycerol. The covered cells on the slide were left for 1 day. Imaging was conducted utilizing an Olympus IX83 inverted microscope, featuring an excitation filter within the wavelength range of BP 330–385 nm and a band absorbance filter positioned below 405 nm. The observations were recorded at a magnification of 20×.

Flow cytometry

Non-cancer cells (NIH3T3) and cancer cells (B16F10, MCF-7) were cultured for 48 h in a 35 mm Petri dish. Subsequently, guanine (500 nM) was incubated with NIH3T3 cells for 12 h. The cells were then washed with PBS to eliminate excess compounds from the cell medium. Following the washing,

the **CuCD** (200 μg mL^{-1}) was incubated in the guanine-treated cell lines for an additional 12 h. Concurrently, the **CuCD** (200 μg mL^{-1}) was also incubated in guanine non-treated NIH3T3, B16F10 and MCF-7 cell lines for 12 h. The cells incubated solely with the **CuCD** and those incubated with both guanine and **CuCD** were detached from the 35 mm Petri dish using trypsin, followed by centrifugation for 5 min. Consequently, the collected cells were resuspended in 500 μL of PBS, and a cytometric analysis was performed. A BD FACS Aria III flow cytometer was utilized to analyze the cells, employing an excitation wavelength of 405 nm.

Results and discussion

Carbon dots (CDs) exhibit notable advantages in biosensing due to their distinctive physicochemical properties, including stable photoluminescence (PL), non-toxicity, and chemical inertness. Their remarkable feature lies in converting abstract information related to target analytes into discernible optical signals, such as changes in fluorescence intensity, wavelength, or color, thereby establishing significance in biosensing.[42] Interestingly, the PL property of CDs can be tuned by selecting appropriate carbon precursors,[43] adjusting synthesis conditions,[44] and introducing heteroatom doping.[45] Doping introduces novel chemical reactivities and potential applications for CDs. Metal atom doping is particularly noteworthy due to its different band structures that make CDs potent nanoprobes for the desired molecule sensing.[46,47] Copper (Cu^{2+}) complexes, along with other transition metals, such as Fe^{2+}, Co^{2+}, and Ni^{2+}, have garnered significant interest owing to their biocompatible properties and oxidative characteristics.[48] The unique features of Cu^{2+} make it particularly intriguing in both biological applications and industrial processes. There are extensive reports on various Cu^{2+} complexes, showcasing various mixed ligand donors or Schiff Base donors.[49] Notably, Cu^{2+} forms strong binding with the guanine nucleobase of DNA.[50,51] Various models describing the binding of Cu^{2+} to DNA have been proposed in the literature.[50,51] One such model suggests a charge transfer type complex, where two adjacent guanine molecules in the same strand act as donors and Cu^{2+} acts as the acceptor. In this configuration, the ion is intercalated between the two G-C pairs. The primary binding sites of Cu^{2+} on the DNA's guanine base are the N7 and O6 of guanine.[50,51] Another model proposes a chelation scenario, where there is a potential interaction between the accessible N7 of guanine and the nearest phosphate group of the same DNA strand, and so forth.[50,51] These proposed binding models depict the affinity of Cu^{2+} with guanine. Guanine, which is a crucial component of DNA, plays a pivotal role in various biological processes, such as mutation, tumorigenesis, and cancer. Therefore, any alteration in its concentration can induce mutations, tumorigenesis and cell death. Hence, the accurate detection of guanine in biological samples is crucial for the early identification of disease indicators and for monitoring the cellular environment.[52] Many researchers have attempted

**Table 1** Literature reported different guanine sensors

Sl no.	Probes	LOD	Response type	References
1	MoS₂-pencil graphite electrode[4]	0.76 mM	Electrochemical sensor	N. Vishnu et al.[4]
2	Self-assembled monolayer (SAM) of 1,8,15,22-tetraaminophthalocyanatonickel(ɪɪ)[8]	3×10^{-8} M	Electrochemical sensor	A. J. Jeevagan et al.[8]
3	Magnesium oxide and multi-walled carbon nanotubes (MgO-MWCNTs-MCPE)[10]	0.92 mM	Electrochemical sensor	K. Chetankumar et al.[10]
4	Dual-emitting ZnCdTe quantum dots[23]	0.076 μmol L⁻¹	Fluorescent sensing	X. Xua et al.[23]
5	TiO₂-graphene nanocomposite[40]	0.15 mM	Electrochemical sensor	Y. Fan et al.[40]
6	Curcumin conjugated nanocapsules using silica nanoparticles[41]	90 μM	Fluorescent sensing	M. Mouslmani et al.[41]
7	Carbon nanodot and Cu²⁺ conjugate[53]	0.67×10^{-8} mol L⁻¹	Fluorescence turn off- turn on	S. Pang et al.[53]
8	An imidazolium-based ionic liquid[54]	45 nM	Electrochemical sensing by cyclic voltammetry	A. Singh et al.[54]
9	Boron-doped graphene (B–G) nanosheets[55]	3.9×10^{-7} mol L⁻¹	Electrochemical sensor	J. Borowiec et al.[55]
10	AgNCs-NFR + Cu²⁺ complex[56]	1.85 μM	Fluorescent sensing	Y. Li et al.[56]
11	Polymer nanoparticles (LCPNPs) composed of terbiumions (Tb³⁺) and citrate(Cit)[57]	100 nM	Fluorescent sensing	D. R. Kumar et al.[57]
12	Oleylamine-capped CuO nanopar-ticles on MWCNTs[58]	0.084 μM	Fluorescent sensing	L. Fu et al.[58]
13	**Cu²⁺ doped carbon dot (CuCD)**	**0.59 nM**	**Fluorescence turn on**	**Present study**

to sense guanine mostly using the electrochemical method[4] and fluorescence method,[53] quantum dot,[23] conjugate systems,[53] ionic liquids,[54] nanosheets,[55] and polymers using transition metals,[56,57] carbon nanotubes,[58] etc. (Table 1). Each method has its advantages and limitations, such as low selectivity, toxicity of components, and short or limited life for electrochemical sensors.

Motivated by these considerations, we endeavored to develop a selective, sensitive, and easily synthesizable nanoprobe for guanine sensing. Our approach involved synthesizing a Cu²⁺-doped carbon dot (CuCD) exhibiting blue emission under UV light irradiation.[59–61] Cu²⁺ was included as an integral component of the synthesized carbon dot to make it a selective sensor for guanine (Scheme 1).

Synthesis and characterization of Cu²⁺-doped carbon dot (CuCD)

Cu²⁺-integrated carbon dot (**CuCD**) preparation involved using the hydrothermal method. The hydrothermal method is a simple bottom-up approach for synthesizing carbon dots. In general, the water solution of the mixtures was enclosed in a Teflon container in an oven and hydrothermally reacted at high pressure and high temperature. The decomposition and polymerization strongly influenced carbon dots derived by the hydrothermal treatment of precursors. Precursors are decomposed into smaller organic compounds, and these organic compounds are then further polymerized into larger molecules, which finally lead to the formation of the carbon
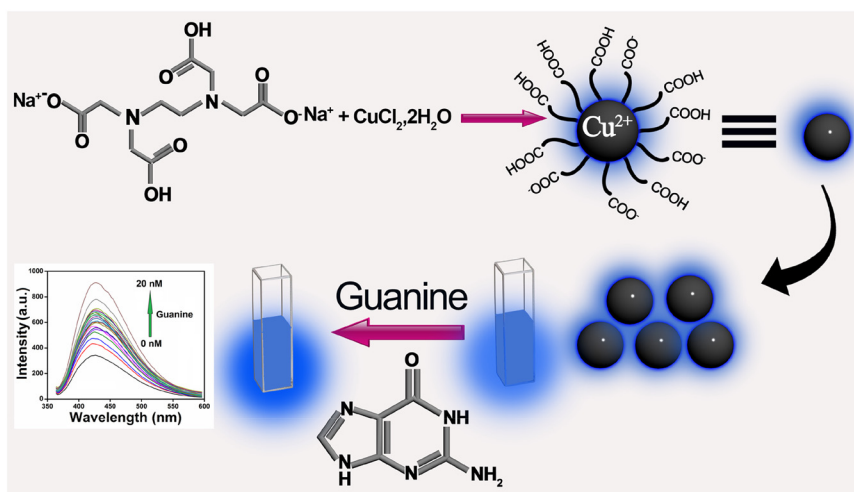
Scheme 1 Schematic representation of guanine sensing by utilizing the intrinsic fluorescence property of Cu²⁺-doped carbon dot (**CuCD**).
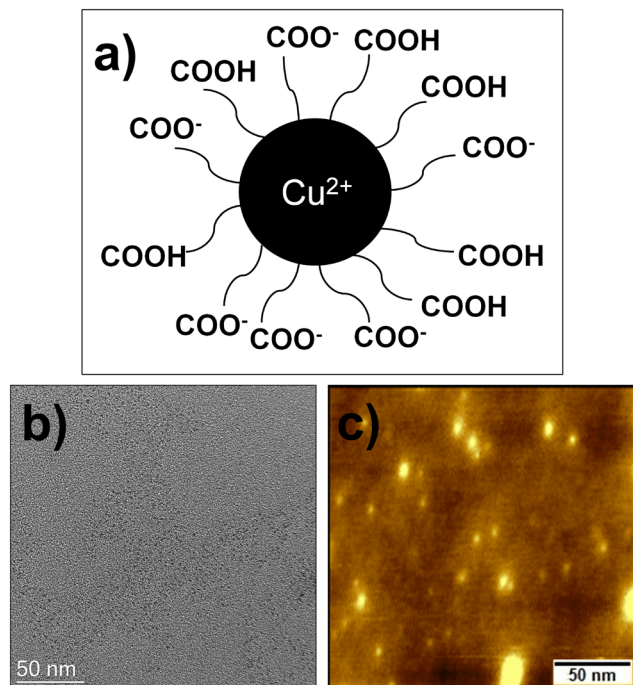
Fig. 1 (a) Chemical structure of **CuCD**, (b) TEM image, and (c) AFM image of **CuCD**.

dots in the hydrothermal reactor. Herein, an equivalent amount of EDTA-2Na, $2H_2O$, and $CuCl_2 \cdot 2H_2O$ was used to prepare the Cu^{2+}-integrated carbon dot (**CuCD**). EDTA-2Na, $2H_2O$ was used as a source of carbon core and carboxylic acid surface functionalization (Scheme S1, (ESI†)) while Cu^{2+} as the doping element (Fig. 1a). We utilized an aqueous saturated solution of the precursors and enclosed it with a Teflon container in an oven with a temperature of 190 °C for 5 h. For control experiments, we prepared another two carbon dots by taking a 1:2 molar ratio and a 2:1 molar ratio of EDTA-2Na, $2H_2O$, and $CuCl_2 \cdot 2H_2O$ (Schemes S2 and S3, ESI†) using identical experimental conditions. The fluorescence intensity for these two carbon dots was significantly low (Quantum yield (QY) ~1–2%). However, the

QY of the carbon dot prepared from a 1:1 molar ratio of EDTA-2Na, $2H_2O$, and $CuCl_2 \cdot 2H_2O$ was observed at ~5%. Thus, we chose the **CuCD**, which was synthesized by an equivalent amount of both precursors because it was more suitable for sensing purposes due to its higher QY. The synthesized **CuCD** was found to be soluble in water, and its corresponding zeta potential (ζ) value was −23.3 mV, suggesting considerable stability in an aqueous medium. Microscopic characterization of the **CuCD** was conducted using TEM and AFM. The TEM images affirmed the size of **CuCD** to be ~5 nm (Fig. 1b). AFM images (Fig. 1c) also indicated that the size of **CuCD** was between 2 and 5 nm, which was similar to the result obtained from the TEM image. In addition, another two FEGTEM high-resolution images of the **CuCD** were captured, where uniformly spherical nanoparticles with diameters of around 5 nm were observed (Fig. S1, ESI†).

In accordance with the microscopic observations, the hydrodynamic diameter of the synthesized **CuCDs** was determined by the DLS study in the solution phase and was found to be around 7–9 nm (Fig. S2, ESI†). The size of **CuCD** was observed to be slightly higher in the DLS study because the nanoparticles were present in the hydrated state, resulting in a hydrodynamic diameter typically larger than the particle diameter determined by TEM and AFM in the dried state. In accordance with the XPS analysis of **CuCD**, peaks at 284, 406, and 529 eV confirmed the presence of C (1s), N (1s), and O (1s) orbitals, respectively (Fig. 2a).

Along with these peaks, a peak with a doublet character was observed in the region of 935–963 eV, corresponding to the presence of Cu in the moiety. The deconvoluted spectra of Cu^{2+} showed two typical peaks at 935.24 eV and 956.02 eV with satellite peaks (943.13 eV and 962.98 eV, respectively) that were associated with Cu $2p_{3/2}$ and Cu $2p_{1/2}$ electronic configurations, respectively, indicating the existence of copper as Cu^{2+} within the **CuCD** (Fig. 2b).[62] We also deconvoluted spectra of C 1s, N 1s and O 1s. A high-resolution XPS spectrum of C 1s can be deconvoluted into four peaks at 283.7, 285.1, 287, and 288.6 eV, which provides
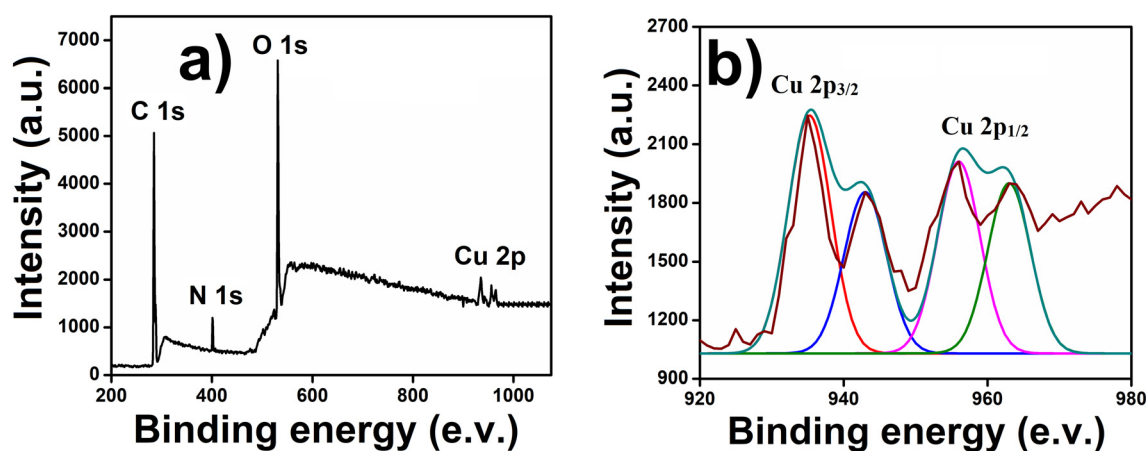

Fig. 2 (a) XPS spectra of **CuCD** and (b) deconvoluted Cu 2p orbital of **CuCD**.

proof of the presence of C=C, C–C, C–N/C–O, and HO–C=O bonds, respectively (Fig. S3a, ESI†). The deconvoluted high-resolution O 1s spectrum of **CuCD** shows three peaks at 530.2, 532.2, and 534.8 eV, which can be attributed to the C=O, C–OH/C–O–C, and O=C–OH groups, respectively (Fig. S3b, ESI†). Two deconvoluted peaks at 399.1 and 401.3 eV in the N 1s level of **CuCD** can be assigned to the C–N–C and N–(C3) bonds, respectively (Fig. S3c, ESI†). The atomic percentages of C1s, N1s, O1s and Cu were 24.02%, 8.92%, 60.8%, and 6.1%, respectively. The XRD analysis was carried out for the characterization of **CuCD**. The presence of peaks in the range of 20–25° confirmed the amorphous nature of **CuCD**, and we also obtained a peak at 49.7°, which confirmed the presence of Cu in the **CuCD** (ref. 63) (Fig. S4a, ESI†). Further, the EDX analysis of **CuCD** corroborated the analysis of XPS that Cu was present in the **CuCD** along with other elements (C, O, and N) (Fig. S4b, ESI†).

UV-vis and fluorescence spectroscopy of CuCD

The UV-visible spectrum of **CuCD** aqueous solution showed one prominent feature centered at 334 nm (Fig. 3a) due to n → π^* transitions attributed to the oxygen containing functional groups. The optical band gap of the **CuCDs** was determined using a Tauc plot derived from the UV-vis spectrum.[64] The optical band gap, E_g, and absorption coefficient, α, are related through the Tauc equation $(\alpha h\upsilon)^{1/n}$ = $B(h\upsilon - E_g)$, where $h\upsilon$ is the photon energy, B is a proportionality constant, n is an exponent that is equal to 1/2 for direct transitions, and Plank's constant (h) = 6.626×10^{-34} Joule s and velocity of light (c) = 2.99×10^8 meter per s. The Tauc plot in Fig. S5† shows the relation between $(\alpha h\upsilon)^{1/2}$ *versus* $h\upsilon$ from which the optical band gap of the **CuCDs** was found to be ~4.22 eV (Fig. S5, ESI†). Such band gap energy illustrates the quantum confinement effect in **CuCDs**.

In the fluorescence study, the **CuCD** showed an excitation-dependent emission. We varied the excitation wavelength from 310 nm to 380 nm and observed a red shift (~29 nm) from 419.7 nm to 448.7 nm in the emission spectra. The **CuCD** showed emission maxima at 423 nm (λ_{max}) upon excitation at 350 nm (Fig. 3b). The aqueous solution of **CuCD** showed bright blue fluorescence (inset, Fig. 3b), which remained consistent with the emission behavior of **CuCD** under UV light irradiation at 365 nm. The excitation
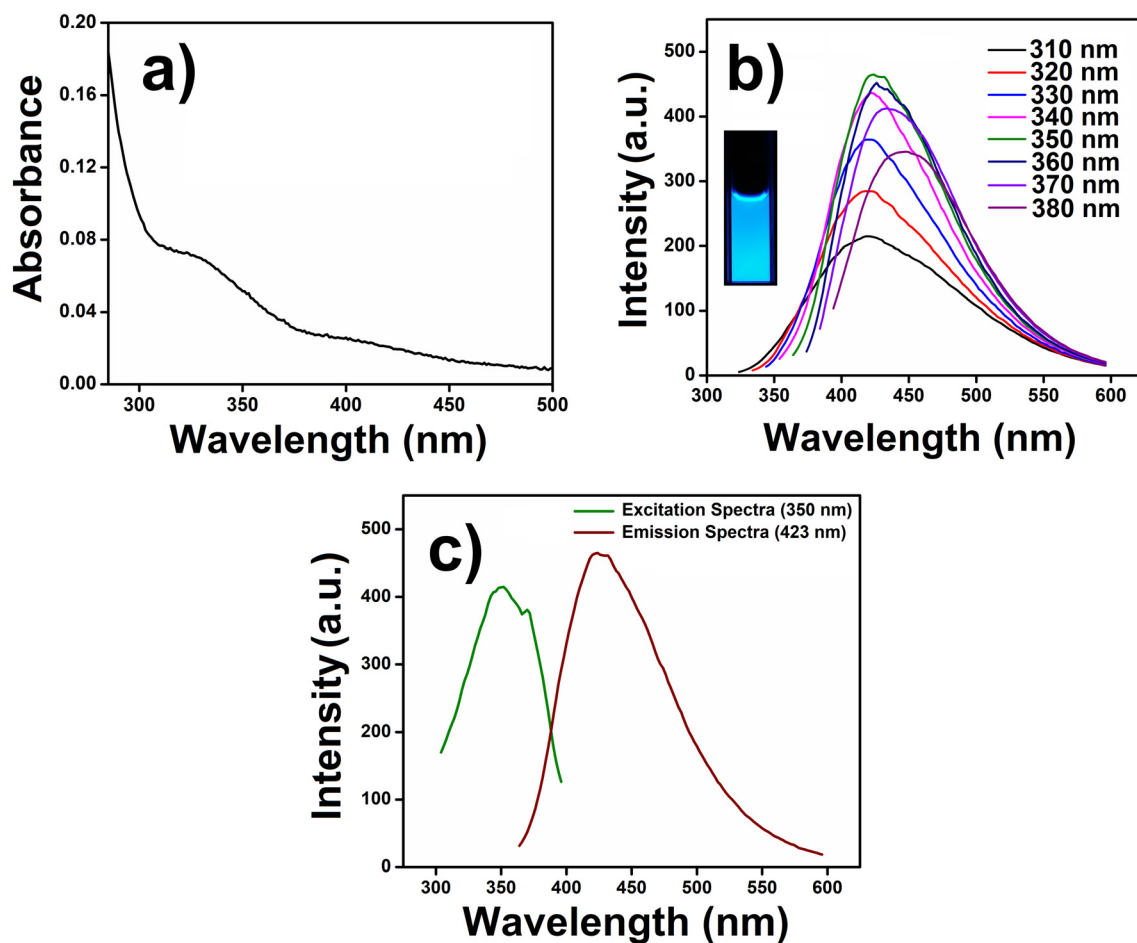

Fig. 3 (a) UV-visible spectrum, (b) excitation-dependent emission spectra of **CuCD** (inset: photographs showing the blue fluorescence of **CuCD** solution under UV irradiation, 365 nm) and (c) excitation spectrum of **CuCD** for λ_{max} (423 nm) alongside the emission spectra.

spectrum (350 nm) of **CuCD** for λ_{max} (423 nm) was plotted along with the emission spectrum (423 nm), as shown in Fig. 3c. The QY of **CuCD** was observed to be around 5% with respect to quinine sulfate. Thus, the intrinsic fluorescence properties of **CuCD** may be explored for the guanine.

Guanine sensing by CuCD

After the successful preparation and photophysical characterization of **CuCD**, we intend to explore its emissive properties in sensing one of the nucleobases of DNA, guanine. Guanine is one of the two essential purine bases of DNA, which plays a major role in coronary blood flow regulation, energy transduction, and cell proliferation; the modulation of its concentration leads to mutation and multiple diseases.[10] For the past decade, nucleobase sensing has been an interesting topic among researchers as DNA, and the key to the genetic materials of all beings was created by these nucleobases (A, T, G, and C). Sensing and investigation of these nucleobases will open a gateway for new domains regarding the diagnosis and treatment of various dreadful diseases. Among all nucleobases, guanine is particularly susceptible to oxidation because it is responsible for many diseases, such as cancer and AIDS. Many researchers have attempted to sense guanine primarily using electrochemical and fluorescence methods. Various materials and techniques have been employed, including quantum dots, conjugate systems, ionic liquids, nanosheets, polymers using transition metals, and carbon nanotubes (Table 1). Each method has unique advantages and limitations. For example, electrochemical sensors often suffer from low selectivity, component toxicity, and limited lifespan. However, the **CuCD** has cost-effective synthesis, low toxicity, high stability and high sensitivity towards guanine. Hence, our objective is to use the intrinsic fluorescence property of **CuCD** for the selective sensing of guanine.

In this regard, the intensity of the fluorescence spectra of **CuCD** (250 μg mL^{-1}) at 423 nm was recorded in the presence of varying concentrations of guanine (0–20 nM). Interestingly, as the concentration of guanine gradually increased, there was a corresponding increase in the emission intensity of **CuCD** (Fig. 4a).

Because the **CuCD** exhibited a sensitive response to guanine, we determined the detection limit of guanine. The emission intensity of **CuCD** (250 μg mL^{-1}) at 423 nm showed a steady increase with the concentration of guanine in the range of 1–20 nM (Fig. 4a). Sensitivity was assessed by examining the relationships between the ratios of the emission intensities of **CuCD** at different guanine concentrations. The fluorescence response curve demonstrated a well-defined linear behavior, as depicted in the plot. $(F - F_0)/F_0$, where F_0 is the emission intensity of the native **CuCD** and F is the emission intensity of **CuCD** in the presence of guanine against the concentration of guanine demonstrated a linear relationship in the concentration range of 1–10 nM, indicating efficient guanine sensing at low concentrations (Fig. 4b). The detection limit of guanine was found to be 0.59 nM for the **CuCD** as determined based on $3\sigma/S$, where σ is the standard deviation and S is the slope of the calibration curve. The linear regression equation was $(F - F_0)/F_0 = 0.059x + 0.2876$, where '$x$' is the concentration of guanine (nM), with a correlation coefficient (R^2) of 0.97. The increase in the fluorescence intensity of **CuCD** by guanine was analyzed quantitatively using the Stern–Volmer equation:

$$F/F_0 = 1 + K_{SV}[Q] \tag{4}$$

In the given equation, F and F_0 represent the fluorescence intensities of **CuCD** in the presence and absence of guanine, respectively. K_{SV} represents the Stern–Volmer constant, and [Q] denotes the concentration of the analyte. The observed change in F/F_0 of **CuCD** with guanine (up to 10 nM) was examined, revealing linearity in the fluorescence intensity increase according to the Stern–Volmer plot with a K_{SV} of 0.059 nM^{-1} (Fig. S6, ESI†).

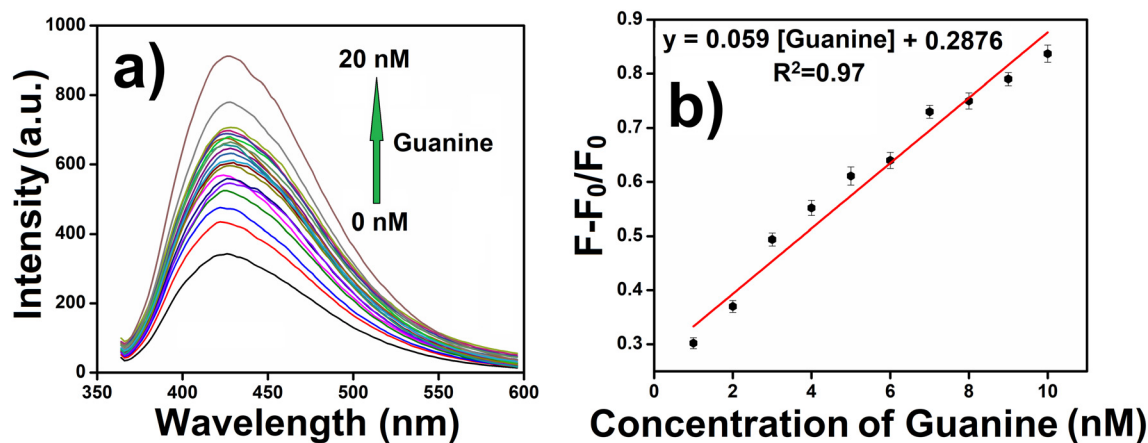**Fig. 4** (a) Fluorescence intensity of **CuCD** (250 μg mL^{-1}) in the presence of guanine (0–20 nM) and (b) fluorescence response of **CuCD** (250 μg mL^{-1}) towards guanine sensing with varying concentrations of guanine (1–10 nM).

This highly sensitive and simple sensing mechanism employed by this **CuCD** for guanine nucleobase is deemed superior in comparison to some previously reported methods (Table 1).

Selective guanine sensing by CuCD

The next obvious intriguing issue is the influence of other nucleobases on the emission property of **CuCD**. Other than guanine (G), DNA has another three nucleobases, *i.e.*, adenine (A), cytosine (C) and thymine (T). We investigated the sensitivity and selectivity of **CuCD** towards other nucleobase bases (A, T, and C). Selectivity is essential and crucial for the credibility of any new sensor. To this end, in different sets of experiments, A, T, and C (500 nM) were separately added to 1 mL of **CuCD** (250 μg mL^{-1}) solution. Interestingly, in comparison to the native emission intensity of **CuCD**, very meager changes (quenching) in the fluorescence intensity of **CuCD** were noted in the presence of very high concentrations (500 nM) of adenine, cytosine and thymine (Fig. 5a). However, the increase in fluorescence intensity in the presence of only 20 nM of guanine was overwhelmingly significant compared to that in the presence of A, T and C (Fig. 5a). In contrast, 500 nM of A, T and C could not influence any significant change in the emission intensity of **CuCD**. A lesser amount of guanine is capable of increasing the emission of **CuCD** far more significantly than that of the 25-times higher concentration of other nucleobases. This observation undoubtedly increases the reliability of the newly developed **CuCD** as a selective and highly sensitive guanine detector, among other nucleobases (Fig. 5a and b).

Molecular sensing always depends on its interaction with a particular sensor. Simultaneously, the specific interaction influences the selectivity of a sensor towards the particular molecule. It is well-established that Cu^{2+} can make strong interactions with Schiff bases, oxygen, nitrogen, and sulphur containing units specially mixed ligand donor type moieties.[47] All the nucleobases of DNA have one of these structural features within them (Fig. S7, ESI†). A, G, and C have Schiff bases, while T has oxygen as a donor ligand in its structure. Within the nucleobases, only adenine (A) and guanine (G) feature Schiff bases as donor ligands. Additionally, guanine employs oxygen, and adenine utilizes nitrogen as additional donor ligands. This configuration enables them to establish a more robust interaction with **CuCD** compared to cytosine (C) and thymine (T). It is interesting that despite having similar structural properties of adenine and guanine, the **CuCD** was more selective towards guanine. According to previous reports, guanine oxygen at C6 and N7 has the perfect arrangement for making suitable interaction with Cu^{2+} of **CuCD**.[48,49,65,66] Primary amine at C2 of guanine can engage in the resonance; consequently, the lone pair of oxygen at C6 could be readily available for creating impactful interactions with Cu^{2+} of **CuCD**. The abundant surface defects of carbon dots play a major role in their optical properties. Upon photoexcitation, rapid charge separation occurs in the carbon dots, leading to the formation of electrons and holes. These charge carriers are 'trapped' at various surface sites, and radiative recombination of the electrons and holes contributes to their intrinsic emission.[66,67] The interaction of carbon dots with the analyte can influence the recombination between the surfaces of electron–hole pairs, thereby affecting the fluorescence properties of carbon dots. A more effective interaction with analytes in carbon dots may stabilize the surface sites for electrons and holes, facilitating efficient radiative recombination, which results in higher fluorescence. Considering these facts, it can be concluded that a possible stronger interaction of guanine with Cu^{2+} doped in carbon dots might have significantly enhanced the emission of **CuCD** (Fig. S8, ESI†).[66,67] Thus, it may be assumed that adenine with primary amine at C6 and N7 has the optimal arrangement for making suitable interaction with
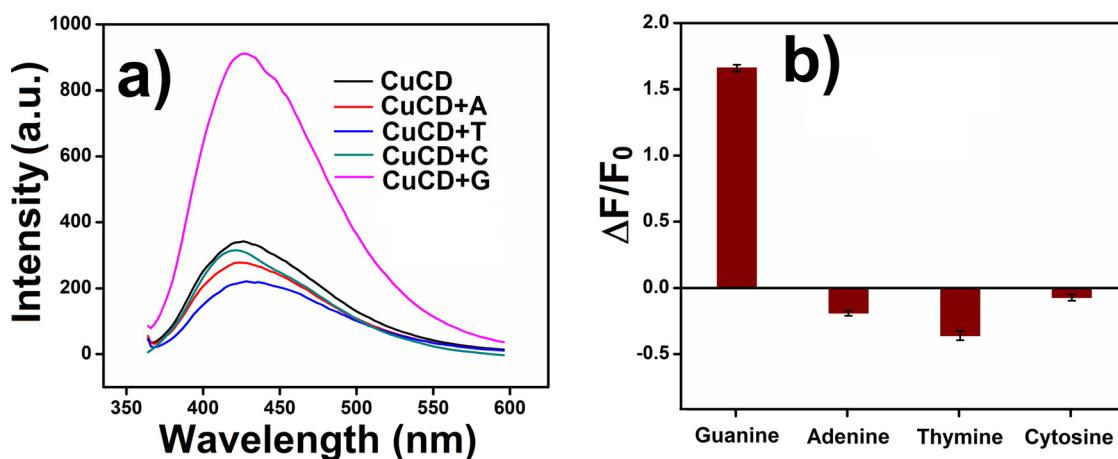

Fig. 5 Selectivity of **CuCD** (250 μg mL^{-1}) to guanine (20 nM) over other nucleobases, adenine (A), cytosine, (C) and thymine (T) (500 nM). (a) Fluorescence intensity plot and (b) relative intensity of **CuCD** in the presence of different nucleobases. The error bars represent the standard deviations.

Cu^{2+} of **CuCD**. However, the lone pair of primary amine at C6 was not available for greater interactions with Cu^{2+} because it was possibly engaged in extended resonance within the ring of adenine (Fig. S7, ESI†). Consequently, Cu^{2+} of **CuCD** could not have a strong interaction with adenine in comparison to that of guanine. Therefore, adenine did not affect the inherent emission intensity of **CuCD**.

Furthermore, an interference study was performed to investigate the selective sensing of guanine even in the presence of other nucleobases. The fluorescence intensities of the **CuCD** (250 µg mL^{-1}) solution in the presence of 20 nM of all the other nucleobases (A, T, and C) were separately recorded in the absence of guanine. As expected, there was no change in the emission intensity of **CuCD** in the presence of A, T and C (Fig. S9, ESI†). Subsequently, guanine (20 nM) was added to each sample of the nucleobase and **CuCD** mixture, and the emission intensities were further recorded. In each case, the fluorescence intensity significantly increased upon the addition of guanine in that mixture (Fig. S9, ESI†). These observations further established that **CuCD** could selectively sense guanine even in the presence of other nucleobases (A, C, and T).

Apart from being a major part of DNA, guanine is also an essential biomolecule for cells. Thus, selective guanine sensing with respect to different monovalent ions, divalent ions, amino acids and biomolecules, which are abundant in the cell environment, is very important. To this end, the fluorescence intensity of **CuCD** (250 µg mL^{-1}) was recorded in the presence of 500 nM (each component) of monovalent ion (Na$^+$ and K$^+$), divalent ion (Ca^{2+}, Fe^{2+}, and Zn^{2+}), amino acids (L-cys, L-trp, L-tyr, L-arg, and L-asp acids) and biomolecules (GSH and H$_2$O$_2$). For monovalent and divalent ions, there were no changes in the fluorescence intensity of **CuCD** with respect to native emission (Fig. S10a and b, ESI†). In the case of amino acids and biomolecules, there were no significant changes in the fluorescence intensity of **CuCD** compared to that in the presence of guanine (20 nM) (Fig. S10a and b, ESI†). L-Arginine among other interferons showed little impact because Cu^{2+} can strongly interact with Schiff bases (C═N–). These results once again affirmed the strong interaction of **CuCD** with guanine compared to all other investigated molecules. Furthermore, we represented the selectivity bar graph of **CuCD**, where the selectivity of guanine with other nucleobases and different metal ions, amino acids, and biomolecules were depicted altogether (Fig.
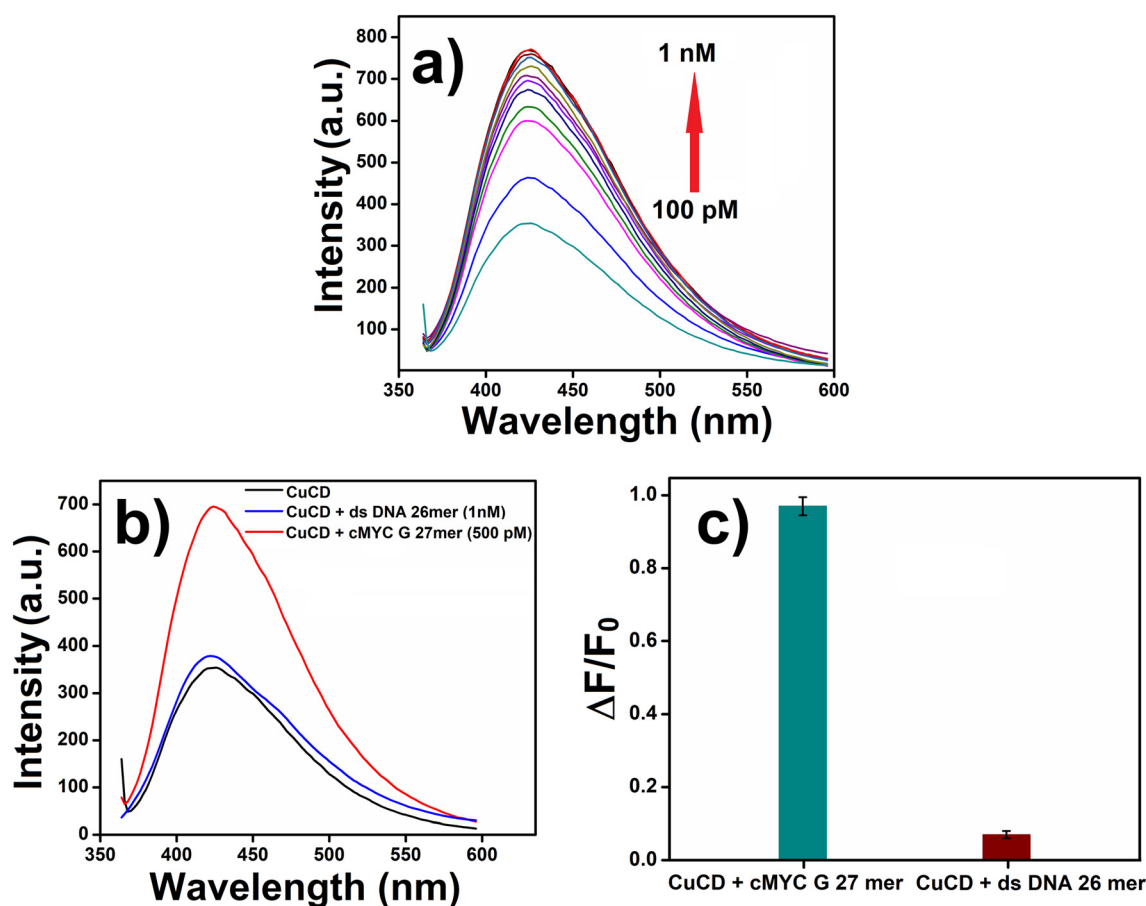
Fig. 6 Fluorescence intensity plot of **CuCD** (250 µg mL^{-1}) in the presence of (a) cMYC G 27mer oligonucleotide (0.1–1 nM). (b) Selectivity and fluorescence intensity plot and (c) relative intensity plot of **CuCD** (250 µg mL^{-1}) in the presence of cMYC G 27mer (500 pM) and ds DNA 26mer (1.0 nM) oligonucleotides. The error bars represent the standard deviations.

S10c†). Therefore, we can certainly assume that the newly synthesized **CuCD** detects guanine with high selectivity and sensitivity against all other DNA nucleobases, different ions, amino acids and biomolecules.

Oligonucleotides are short DNA or RNA molecules, that have a wide range of applications in bio-medical research. Desired oligonucleotides can be prepared by modifying the precursor nucleotides. These modifications give new properties to the oligonucleotides and make them key elements in diverse research domains. Herein, we used two oligonucleotides: cMYC G 27mer and ds DNA 26mer. cMYC G 27mer (DTGGGGAGGGTGGGGAGGGTGGGGAAGG) was the guanine-enriched oligonucleotide, and ds DNA 26mer (DCAATCGGATCGAATTCGATCCGATTG) was the control oligonucleotide. A stock solution (100 μM) of both oligonucleotides was prepared. Subsequently, we investigated the fluorescence intensity of **CuCD** (250 μg mL^{-1}) in the presence of cMYC G 27mer (0.1–1.0 nM). Interestingly, with increasing concentrations of cMYC G 27mer, the fluorescence intensity of **CuCD** gradually increased (Fig. 6a). Additionally, we carried out a similar experiment on the fluorescence property of **CuCD** in the presence of both cMYC G 27mer (500 pM/0.5 nM) and ds DNA 26mer (1.0 nM). The fluorescence intensity of **CuCD** increased in the presence of cMYC G 27mer but remained unchanged in the presence of ds DNA 26mer (Fig. 6b and c). Guanine enrichment in the cMYC G 27mer oligonucleotide made it susceptible to the **CuCD** to influence its emission property more significantly in contrast to the control oligonucleotide, ds DNA 26mer. These observations further validated the utilization of **CuCD** as a potential biomarker that is highly specific to guanine.

IR spectra study

After highly sensitive and selective sensing of guanine by **CuCD**, we investigated the change in the vibrational frequency of **CuCD** in the presence of guanine using IR

spectra. The IR spectrum of **CuCD** showed O–H stretching of the –COOH group at around 3445 cm^{-1}, and a sharp –C=O spectrum for the –COOH group merged with the C=C bending of alkyne at 1636 cm^{-1} and the O–H bending of the –COOH group at 1384 cm^{-1} (Fig. 7(i)). The above frequency peaks in the IR spectrum of **CuCD** indicate the presence of carboxylic acid on the surface of the newly synthesized carbon dot. Next, we investigated the IR spectra of **CuCD** in the presence of guanine. The FTIR spectrum of the **CuCD**-guanine complex showed O–H stretching of the –COOH group at around 3436 cm^{-1}, and the sharp peak due to the presence of –C=O frequency for the –COOH group was split into two peaks. One was at 1652 cm^{-1} in the presence of a –C=O bond and another at 1580 cm^{-1} possibly due to the rise of a complex formation between –C=N– of guanine and Cu^{2+}.[49] The peak at 1393 cm^{-1} was sharper than the peak of **CuCD** possibly due to the merging of the different vibrational frequencies of the heterocyclic ring of guanine along with the frequency of the O–H bond of the –COOH group. The peak at 890 cm^{-1} in the spectrum of **CuCD** in the presence of guanine may arise from the bond formation between Cu^{2+} and guanine, which was not properly visible only in the **CuCD** spectrum (Fig. 7).[68] These characteristic peaks in the FTIR spectra conclude that the **CuCD** successfully formed a complex with guanine, resulting in a dramatic increase in the fluorescence intensity of **CuCD**. Moreover, we carried out a FEGTEM microscopic experiment of the **CuCD**-guanine complex to find out if there was any change in the microscopic property of carbon dots (Fig. S11, ESI†). The FEGTEM image of the **CuCD**-guanine complex showed assimilating structures of carbon dots (Fig. S11b and d, ESI†) in comparison to the dispersed FEGTEM image of the **CuCD** (Fig. S11a and c, ESI†). A high-resolution FEGTEM image showed the presence of big size particles along with small size carbon dots in the assimilated structure, which may be proof of the formation of the **CuCD**-guanine complex (Fig. S11d†). This type of assimilating structure along with the different size particles was absent in the FEGTEM image of only **CuCD** (Fig. S11c†). Hence, in the presence of guanine, the **CuCD** forms a complex that might have facilitated the increase in the fluorescence intensity of **CuCD**, thereby sensing the guanine.

Media stability of CuCD

Before deploying the newly synthesized **CuCD**, as a potential bioprobe for guanine sensing in a cellular environment, we conducted an assessment of its (i) stability in biological media over time and (ii) cytocompatibility with mammalian cells. In FBS-DMEM media, 500 μg mL^{-1} of **CuCD** was introduced with varying concentrations of FBS (up to 75%) and incubated for 48 h (Fig. S12a, ESI†). The prolonged stability of **CuCD** was also evaluated by maintaining mixtures of **CuCD** (500 μg mL^{-1})-FBS (10%)-DMEM media for 10 days (Fig. S12b, ESI†). In both cases, the suspension stability index (SSI) of **CuCD** in the media was approximately 90 ± 2% for
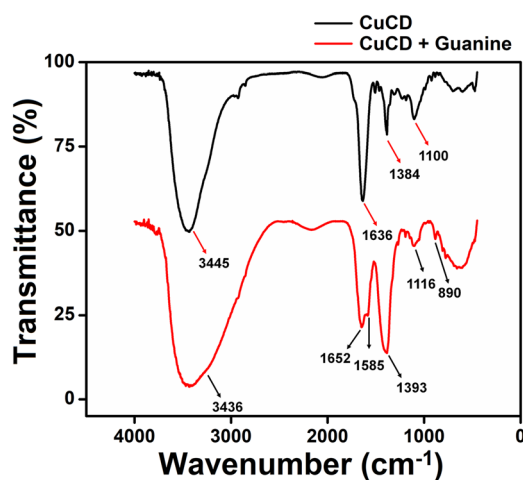

Fig. 7 FTIR spectrum of **CuCD** and **CuCD** in the presence of guanine.

different concentrations of FBS (0–75%), (Fig. S12a and b, ESI†). The stability of **CuCD** in biological media was corroborated by visual images (Fig. S12a, ESI†). Furthermore, we examined the stability of **CuCD** under UV light exposure (365 nm and 12 W), where no photobleaching property was observed, and the emission characteristics of the fluorescent bioprobes remained unchanged even after 200 min of UV irradiation (Fig. S12c, ESI†).

Cytocompatibility of CuCD

After confirming the stability of **CuCD** in the biological milieu, we investigated the cytocompatibility of **CuCD** against mammalian cells with the aim of utilizing this bioprobe for cellular imaging and guanine detection inside cells. We assessed the cytocompatibility of **CuCD** within B16F10, MCF-7 and NIH3T3 cells using MTT assay. Various concentrations of **CuCD** (25–200 μg mL^{-1}) were incubated with B16F10 melanoma cells, MCF-7 breast cancer cells and noncancerous NIH3T3 cells. Remarkably, the results indicated that the cell viability of **CuCD** was approximately 85% for all the investigated mammalian cells after 12 h of incubation. (Fig. S13, ESI†).

Bioimaging

Detecting guanine in the cellular environment is crucial for the early diagnosis of various diseases and for monitoring human health.[10] Disruptions in the normal levels of guanine within nucleic acids can lead to deficiencies and mutations

in the immune system, potentially contributing to a range of diseases such as carcinoma, Parkinson's disease, epilepsy, and liver diseases.[50] Therefore, we aimed to exploit the fluorescence property of **CuCD** in bioimaging. The observed increase in the fluorescence intensity of **CuCD** in the presence of guanine also prompted us to delve deeper into utilizing this probe to distinguish between guanine-enriched cells and the respective control cells. In this search, we identified G-quadruplexes (G4s), which are non-canonical secondary structures found in DNA and RNA sequences rich in guanine, as potential targets for investigation.[69] They play crucial roles in cancer development and progression. G4s consist of two or more planar G-tetrads held together by Hoogsteen hydrogen bonds and pi-stacking.[69] They are associated with telomere shortening, DNA replication, and the expression of oncogenes and proto-oncogenes.[69] The presence of G4s is linked to genomic instability and carcinogenesis, with a significant association with oncogenes and tumor suppressors. G4s have become attractive targets for gene regulation, and various small molecules are being explored even in clinical trials because of their potential to target G4s in oncogene promoters.[69] Considering this guanine-enriched G4 structure, we planned to diagnose two cancer cell lines, B16F10 and MCF-7, that have overexpressed G4[69,70] against the noncancer cell line NIH3T3 with and without guanine incubation by investigating the change in the fluorescence of **CuCD**.

Native fluorescence, also known as autofluorescence (AF), occurs when biological substrates emit light in the UV-visible
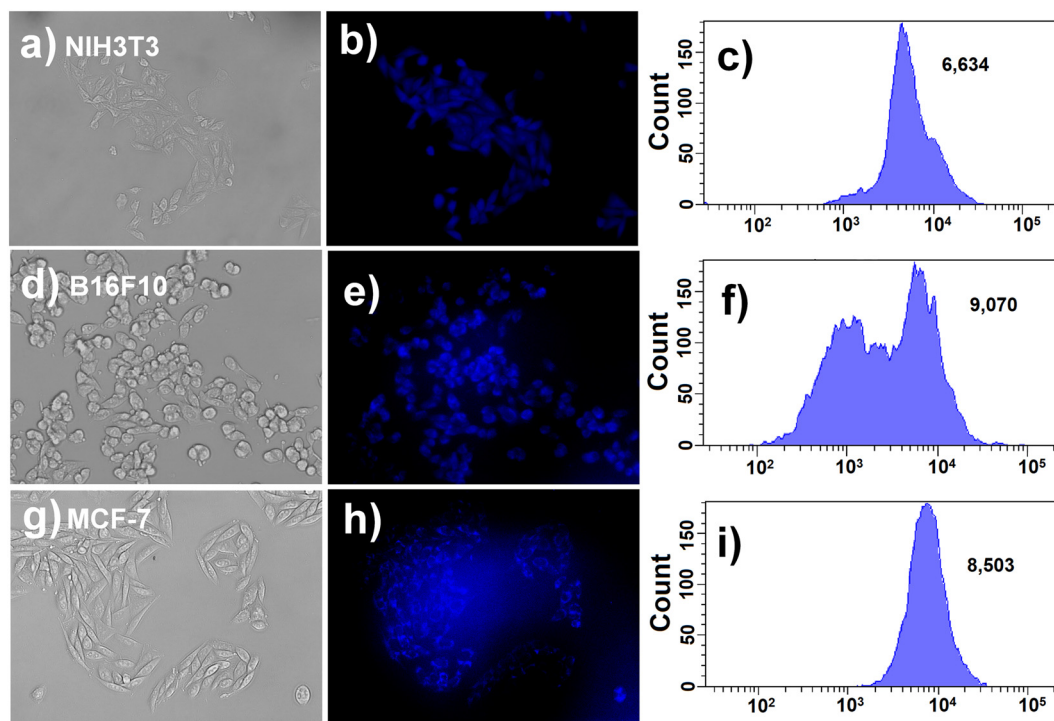
Fig. 8 Bright field and fluorescence microscopic images of cells after 12 h incubation with **CuCD** where [**CuCD**] = 200 μg mL^{-1} in the case of (a and b) untreated NIH3T3, and (c) corresponding mean fluorescence intensity; (d and e) B16F10 and (g and h) MCF-7 (f and i) corresponding mean to fluorescence intensity for B16F10 and MCF-7, respectively.

or near-IR spectral range upon excitation with suitable wavelengths of light. The **CuCD** exhibits fluorescence when excited at 350 nm. Following the incubation of **CuCD** in various cell lines, we initially examined the cells under fluorescence microscopy. Subsequently, upon capturing images of the cell lines incubated with **CuCD**, we performed background subtraction to generate the final **CuCD**-incubated cell line images. This process effectively eliminated the autofluorescence present in the image background, resulting in clear cell images exhibiting blue fluorescence.

In this context, we incubated guanine (500 nM) with NIH3T3 cell lines for 12 h. After 12 h, the guanine-incubated NIH3T3 cell line was washed three times with PBS. Then, guanine-treated NIH3T3 and guanine-non-treated NIH3T3 cells were incubated with **CuCD** (200 μg mL^{-1}) for 12 h. In addition, the G4-enriched B16F10 and MCF-7 cell lines were incubated with **CuCD** (200 μg mL^{-1}) for 12 h. Following the incubation period, both guanine-treated and -non-treated cells NIH3T3 and B16F10, and MCF-7 were examined under a fluorescence microscope. Notably, guanine-treated NIH3T3 cells displayed vivid blue fluorescence, indicating internalized **CuCD** (Fig. S14a and b, ESI†) with a mean fluorescence intensity of 11 235 (Fig. S14c, ESI†). In contrast, comparatively poor fluorescence was observed in guanine-non-treated NIH3T3 cells (Fig. 8a and b) with a mean fluorescence intensity of 6634 (Fig. 8c) under identical experimental conditions. Interestingly, in the case of G4-enriched B16F10 (Fig. 8d and e) and MCF-7 cells (Fig. 8g and h), bright blue fluorescence of internalized **CuCD** was observed with mean fluorescence intensities of 9070 (Fig. 8f) and 8500, respectively, (Fig. 8i) without the addition of any external guanine. The difference between the mean fluorescence intensity of the observed cellular internalized **CuCD** in guanine-treated NIH3T3 cells and G4-enriched B16F10 and MCF-7 cells compared to that of guanine-non-treated NIH3TE cell lines demonstrated its utility as a potential biomarker for guanine nucleobase both *in vitro* and within mammalian cells.

Conclusion

In this work, we synthesized a Cu^{+2}-doped carbon dot (**CuCD**) using the hydrothermal method, which exhibited excitation-dependent blue fluorescence at 423 nm when excited at 350 nm. All microscopic and spectroscopic characterizations were carried out for this newly synthesized **CuCD**. The size of the synthesized **CuCD** was found to be ~5 nm, as observed from TEM, AFM and DLS. XPS confirmed the presence of Cu^{2+} in the **CuCD**. The **CuCD** can efficiently detect the guanine nucleobase through the enhancement of its intrinsic fluorescence with a limit of detection of 0.59 nM. The formation of a complex with a guanine nucleobase by the **CuCD** was substantiated by FTIR spectroscopy. This Cu^{+2}-doped carbon dot can also selectively detect guanine with high sensitivity against other nucleobases of DNA (A, T and C) and with respect to

monovalent and divalent ions, amino acids and biomolecules. The selective affinity of **CuCD** for guanine was also observed particularly in a guanine-enriched oligonucleotide, cMYC G 27-mer (DTGGGGAGGGTGGGGAGGGTGGGGAAGG) in contrast to oligonucleotide, dsDNA 26-mer (DCAATCGGATCGAATTCGATCCGATTG) devoid of high guanine content. Concurrently, the **CuCD** was successfully employed for bioimaging guanine-enriched B16F10, MCF-7 cells and guanine-treated NIH3T3 cell lines *via* an increase in fluorescence intensity within living cells with respect to guanine non-treated NIH3T3 cells. Hence, the **CuCD** can be used as a selective and sensitive diagnostic probe for guanine sensing both *in vitro* and within mammalian cells.

Data availability

The data supporting this article have been included as part of the ESI.†

Author contributions

Conflicts of interest

The authors declare that they have no known competing financial interests or personal relationships that could have appeared to influence the work reported in this paper.

Acknowledgements

References

1 A. H. Kamel, F. T. C. Moreira, C. Delerue-Matos and M. G. F. Sales, *Biosens. Bioelectron.*, 2008, **24**, 591–599.

2 D. Wang, B. Huang, J. Liu, X. Guo, G. Abudukeyoumu, Y. Zhang, B. Ye and Y. Li, *Biosens. Bioelectron.*, 2018, **102**, 389–395.

3 E. Palecek, *Bioelectrochem. Bioenerg.*, 1986, **15**, 275–295.

4 N. Vishnu and S. Badhulika, *Biosens. Bioelectron.*, 2019, **124-125**, 122–128.

5 K. L. Ng and S. M. Khor, *Anal. Chem.*, 2017, **89**, 10004–10012.

6   I. Hirao, M. Kimoto and R. Yamashige, *Acc. Chem. Res.*, 2012, **45**, 2055–2065.

7   J. G. Wetmur, *Crit. Rev. Biochem. Mol. Biol.*, 1991, **26**, 227–259.

8   A. J. Jeevagan and S. A. John, *Anal. Biochem.*, 2012, **424**, 21–26.

9   W. Saenger and C. R. Cantor, *Principles of nucleic acid structure*, Springer, New York, 1984.

10 K. Chetankumar, B. E. Kumara Swamy and H. S. Bhojya Naik, *Mater. Chem. Phys.*, 2021, **267**, 124610.

11 S. S. Wallace, *Free Radical Biol. Med.*, 2002, **33**, 1–14.

12 X. Wang, J. Zhang, Y. Wei, T. Xing, T. Cao, S. Wu and F. Zhu, *Analyst*, 2020, **145**, 1933–1942.

13 A. Ferancova, S. Rengaraj, Y. Kim, J. Labuda and M. Sillanpaa, *Biosens. Bioelectron.*, 2010, **26**, 314–320.

14 M. Arvand, N. Ghodsi and M. A. Zanjanchi, *Biosens. Bioelectron.*, 2016, **77**, 837–844.

15 S. Jesny, S. Menon and K. G. Kumar, *RSC Adv.*, 2016, **6**, 75741–75748.

16 C. C. Marvel, J. Delrowe, E. G. Bremer and J. R. Moskal, *Mol. Chem. Neuropathol.*, 1994, **21**, 353–368.

17 C. Li and H. Wang, *J. Chromatogr. A*, 2015, **1406**, 324–330.

18 P. Graven, M. Tambalo, L. Scapozza and R. Perozzo, *Exp. Parasitol.*, 2014, **141**, 28–38.

19 G. Chen, Q. C. Chu, L. Y. Zhang and J. N. Ye, *Anal. Chim. Acta*, 2002, **457**, 225–233.

20 B. D. Gill and H. E. Indyk, *Int. Dairy J.*, 2007, **17**, 596–605.

21 F. Yang, J. Guan and S. P. Li, *Talanta*, 2007, **73**, 269–273.

22 Y. Huang and H. Chang, *Anal. Chem.*, 2007, **79**, 4852–4859.

23 X. Xua, L. Hea, Y. Longa, S. Pana, H. Liu, J. Yangc and X. Hu, *Sens. Actuators, B*, 2019, **279**, 44–52.

24 L. Zou, Y. Li and B. Ye, *Microchim. Acta*, 2011, **173**, 285–291.

25 X. Li, X. Gao, W. Shi and H. Ma, *Chem. Rev.*, 2014, **114**, 590–659.

26 Y. Xu, W. Shi, X. He, X. Wu, X. Li and H. Ma, *Anal. Chem.*, 2017, **89**, 10980–10984.

27 G. Li, *Nano-inspired biosensors for protein assay with clinical applications*, Elsevier, United Kingdom, 2019.

28 Z. Wang, X. Xiao, T. Zou, Y. Yang, X. Xing, R. Zhao, Z. Wang and Y. Wang, *Nanomaterials*, 2019, **9**, 32.

29 V. Gubala, G. Giovannini, F. Kunc, M. P. Monopoli and C. J. Moore, *Cancer Nanotechnol.*, 2020, **11**, 1–43.

30 B. H. Lee, S. Suresh and A. Ekpenyong, *J. Biophotonics*, 2018, **12**, e201800172.

31 G. Yang, S. Z. F. Phua, A. K. Bindra and Y. Zhao, *Adv. Mater.*, 2019, **31**, 1805730.

32 S. N. Baker and G. A. Baker, *Angew. Chem., Int. Ed.*, 2010, **49**, 6726–6744.

33 S. Sarkar, K. Das and P. K. Das, *ACS Sustainable Chem. Eng.*, 2017, **5**, 8356–8369.

34 K. K. R. Datta, G. Qi, R. Zboril and E. P. Giannelis, *J. Mater. Chem. C*, 2016, **4**, 9798–9803.

35 B. D. Mansuriya and Z. Altintas, *Nanomaterials*, 2021, **11**, 2525.

36 J. C. G. Esteves da Silva and H. M. R. Gonçalves, *TrAC, Trends Anal. Chem.*, 2011, **30**, 1327–1336.

37 F. Ahmed, S. Iqbal, L. Zhao and H. Xiong, *Anal. Chim. Acta*, 2021, **1183**, 338977.

38 F. Ahmed, S. Iqbal and H. Xiong, *Environ. Sci.: Nano*, 2022, **9**, 2624–2637.

39 F. Ahmed, W. Xu, M. M. Hussain, W. U. Khan and H. Xiong, *Chem. Eng. J.*, 2023, **477**, 147300.

40 Y. Fan, K. J. Huang, D. J. Niu, C. P. Yang and Q. S. Jing, *Electrochim. Acta*, 2011, **56**, 4685–4690.

41 M. Mouslmani, K. H. Bouhadir and D. Patra, *Biosens. Bioelectron.*, 2015, **68**, 181–188.

42 C. Ji, Y. Zhou, R. M. Leblanc and Z. Peng, *ACS Sens.*, 2020, **5**, 2724–2741.

43 J. Ge, Q. Jia, W. Liu, L. Guo, Q. Liu, M. Lan, H. Zhang, X. Meng and P. Wang, *Adv. Mater.*, 2015, **27**, 4169–4177.

44 E. Loi, R. W. C. Ng, M. M. F. Chang, J. F. Y. Fong, Y. H. Ng and S. M. Ng, *Luminescence*, 2017, **32**, 114–118.

45 L. Jiang, H. Z. Ding, S. Y. Lu, T. Geng, G. J. Xiao, B. Zou and H. Bi, *Angew. Chem., Int. Ed.*, 2020, **59**, 9986–9991.

46 M. Vázquez-González, W. C. Liao, R. Cazelles, S. Wang, X. Yu, V. Gutkin and I. Willner, *ACS Nano*, 2017, **11**, 3247–3253.

47 J. Du, Y. Zhao, J. Chen, P. Zhang, L. Gao, M. Wang, C. Cao, W. Wen and C. Zhu, *RSC Adv.*, 2017, **7**, 33929–33936.

48 T. Y. Han, T. S. Guan, M. A. Iqbal, R. A. Haque, K. S. Rajeswari, M. B. K. Ahamed and A. M. S. A. Majid, *Med. Chem. Res.*, 2014, **23**, 2347–2359.

49 S. Jaina, T. A. Khana, Y. P. Patil, D. Pagariya, N. Kishore, S. Tapryal, A. D. Naike and S. G. Naik, *J. Photochem. Photobiol., B*, 2017, **174**, 35–43.

50 I. Sissoeff, J. Grisvard and E. Guillé, *Prog. Biophys. Mol. Biol.*, 1976, **31**, 165–199.

51 V. Andrushchenko, J. H. Van De Sande and H. Wieser, *Biopolymers*, 2003, **72**, 374–390.

52 S. Pradhan, S. Biswas, D. K. Das, R. Bhar, R. Bandyopadhyay and P. Pramanik, *New J. Chem.*, 2018, **42**, 564–573.

53 S. Pang, Y. Zhang, C. Wu and S. Feng, *Sens. Actuators, B*, 2016, **222**, 857–863.

54 A. Singh, A. Singha and N. A. Singh, *Dalton Trans.*, 2014, **43**, 16283.

55 J. Borowiec and J. Zhang, *J. Electrochem. Soc.*, 2015, **162**, B332–B336.

56 Y. Li and J. Liu, *Analyst*, 2020, **145**, 6753–6768.

57 D. R. Kumar, D. Manoj and J. Santhanalakshmi, *Sens. Actuators, B*, 2013, **188**, 603–612.

58 L. Fu, L. Yan, G. Wang, H. Ren and L. Jin, *Talanta*, 2019, **193**, 161–167.

59 Q. Xu, J. Wei, J. Wang, Y. Liu, N. Li, Y. Chen, C. Gao, W. Zhangd and T. Sreeprasede, *RSC Adv.*, 2016, **6**, 28745–28750.

60 J. Guo, W. Lu, H. Zhang, Y. Meng, F. Du, S. Shuang and C. Dong, *Sens. Actuators, B*, 2021, **330**, 129360.

61 Y. Wang, J. Yao, Z. Cao, P. Fu, C. Deng, S. Yan, S. Shi and J. Zheng, *Chem. – Eur. J.*, 2022, **28**, e202104174.

62 J. Wang, M. Xu, D. Wang, Z. Li, F. L. Primo, A. C. Tedesco and H. Bi, *Inorg. Chem.*, 2019, **58**, 13394–13402.

63 M. Najaflu, M. Shahgolzari, F. Bani and A. Y. Khosroushahi, *ACS Omega*, 2022, **7**, 34573–34582.

64 M. Masteri-Farahani and F. Askari, *Spectrochim. Acta, Part A*, 2019, **206**, 448–453.

65 D. X. Xing, X. J. Tan, X. B. Jiang and B. Wang, *Comput. Theor. Chem.*, 2011, **963**, 490–496.

66 Y. Liu, P. Wang, K. A. S. Fernando, G. E. LeCroy, H. Maimaiti, B. A. Harruff-Miller, W. K. Lewis, C. E. Bunker, Z. L. Houa and Y. P. Sun, *J. Mater. Chem. C*, 2016, **4**, 6967–6974.

67 J. Zuo, T. Jiang, X. Zhao, X. Xiong, S. Xiao and Z. Zhu, *J. Nanomater.*, 2015, 787862.

68 Y. Liu, P. Wu, X. Wu, C. Ma, S. Luo, M. Xu, W. Li and S. Liu, *Talanta*, 2020, **210**, 120649.

69 U. Bhatt, A. L. Kretzmann, A. Guedin, A. Ou, S. Kobelke, C. S. Bond, C. W. Evans, L. H. Hurley, J. L. Mergny, K. S. Iyer, A. H. Fox and N. M. Smith, *Biochimie*, 2021, **190**, 124–131.

70 U. Chilakamarthi, D. Koteshwar, S. Jinka, N. V. Krishna, K. Sridharan, N. Nagesh and L. Giribabu, *Biochemistry*, 2018, **57**, 6514–6527.